SIMULATION OF TURBULENT AND THERMAL MIXING IN T-JUNCTIONS USING URANS AND SCALE-RESOLVING TURBULENCE MODELS IN ANSYS CFX

Th. Frank[*], M. Adlakha[*], C. Lifante[*], H.-M. Prasser[**], F. Menter[*]

[*]*ANSYS Germany GmbH, Staudenfeldweg 12, D-83624 Otterfing, Germany*
[**]*ETH Zürich, Dept. Energy Technology, Zürich, Switzerland*

Abstract

Being of importance for turbulent and thermal mixing and consequently for thermal striping and thermal fatigue problems in nuclear power plants, the turbulent isothermal and thermal mixing phenomena have been investigated in two different testcase scenarios. First testcase scenario as proposed by ETHZ, Prasser et al. [18] comprises of turbulent mixing of two water streams of equal temperature in a T-junction of 50mm pipes in the horizontal plane and thereby excluding any buoyancy effects. The second testcase is based on the Vattenfall test facility in the Älvkarleby laboratory and has been proposed by Westin et al. [16], where water of 15K temperature difference mixes in a T-junction in vertical plane, provoking thermal striping phenomena. ANSYS CFX 11.0 with Reynolds averaging based (U)RANS turbulence models (SST, BSL RSM) as well as with scale-resolving SAS-SST turbulence model has been applied to both test cases. The CFD simulations have been carried out in accordance with Best Practice Guidelines as far as they were applicable. Results have been compared to wire-mesh sensor, LDV and thermocouple measurements. While the turbulent mixing in the ETHZ testcase could be reproduced in good quantitative agreement with data, the results of the LES-like simulations were not yet fully satisfying in terms of the obtained accuracy in comparison to the detailed measurement data, also the transient thermal striping phenomena and large-scale turbulence structure development was well reproduced in the simulations.

Introduction

Turbulent mixing of fluid of different temperature in T-junction geometries became of significant importance in the field of nuclear reactor safety, since it can lead to highly transient temperature fluctuations at the adjacent pipe walls, cyclic thermal stresses in the pipe walls and consequently to thermal fatigue and failure of the pipeline. Thermal striping and mixing, in general, is however challenging to predict by using common CFD simulation and turbulence modeling approaches.

Besides the effort spent in former studies for thermal mixing phenomena in T-junctions of the Superphenix reactors, IAEA benchmarks and the European THERFAT project, recently two series of experiments have been carried out, which are directly aimed to provide detailed experimental data for thoroughly validation of CFD simulation approaches for the turbulent mixing of fluids of the same temperature as well as for the thermal striping phenomena in turbulent thermal fluid mixing in T-junctions. The first experiment was carried out by Vattenfall in 2006 at the Älvkarleby laboratory, Vattenfall Research and Development AB, while the second series of detailed measurements of turbulent isothermal and thermal mixing was carried out at the Laboratory for Nuclear Energy Systems, Institute for Energy Technology, ETHZ, Zürich, Switzerland. Both datasets were used in the present work for CFD model validation.

The present paper describes first the Best Practice Guidelines related investigations on the turbulent mixing of water of equal temperature in a T-junction in the horizontal plane (ETHZ testcase, [18]). The investigations were aimed on investigation of grid independent CFD solutions for traditional RANS/URANS approaches using SST and BSL RSM turbulence models.

Furthermore it is easy to observe that these traditional RANS/URANS turbulence modeling approaches are not capable to describe the phenomenon of thermal striping and high-frequency near-wall temperature fluctuations in turbulent thermal mixing in T-junctions correctly. Therefore, based on the experiences from the first testcase investigations, the scale-resolving SAS-SST model has been applied in a transient simulation to the conditions of the Vattenfall test facility [16] for one particular set of testcase conditions. For both testcases a short description of the test facilities and the testcase conditions are given. The detailed mesh and setup parameters for the CFD simulations are described and the CFD results are compared to the experimental data. From that comparison conclusions are formulated for the advantages and disadvantages of the used modeling approaches and recommendations for further investigations are given.

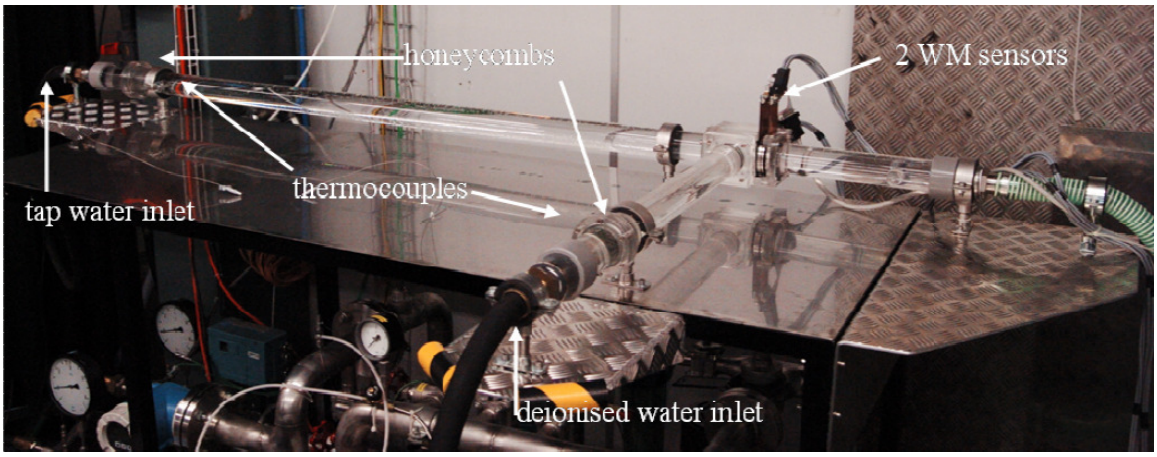

Figure 1: ETHZ T-junction test facility in the horizontal plane.

Flow rate in main pipe (tap water)	58.6 [l/min]
Flow rate in branch pipe (de-ionized water)	59.2 [l/min]
Average velocity in main pipe	~0.5 [m/s]
Average velocity in branch pipe	~0.5 [m/s]
Water temperature	25.0 [°C]

Table 1: Main parameters of the ETHZ T-junction testcase No. 14.

1. ETHZ Testcase – Turbulent Mixing of Isothermal Flows

1.1. ETHZ T-Junction Test Facility

A series of detailed measurements of turbulent isothermal and thermal mixing was carried out at the Laboratory for Nuclear Energy Systems, Institute for Energy Technology, ETHZ, Zürich, Switzerland [18]. The used test section consists of a horizontal T-junction geometry of Plexiglas pipes of 50 mm inner diameter for both the main and the branch pipes. A photo of the test section is given in Fig.1. In the longer run pipe (main pipe, L_M=1.5 m), tap water is flowing from left to right and the deionised water flows from the side through the shorter branch pipe (L_B=0.5 m) as indicated in Fig 1. The two flows join and mix at and after the T-junction and the mixture is drained through a flexible hose shown on the right side (green).

The lengths of the run and branch pipes allow to have a developed flow profile as the fluids arrive to the T-junction. Besides, at beginning of both the run pipe and the branch pipe, just behind the inlets, honeycombs are installed to straighten the flow against any upstream influence. The honeycombs have a cell size of 3.5 mm and a length of 60 mm in flow direction. In the arrangement shown on Fig 1, the main instrumentation, two wire-mesh sensors (WMS), are

installed right behind each other downstream of the T-junction in the mixing region. Three-dimensional flow field measurements (concentration of de-ionized water) have been carried out by the use of the 16×16 electrode WMS on the basis of difference in liquid conductivities of de-ionised and tap water. Applying distance flanges, the sensors can be also positioned further downstream of the T-junction. In the experiments the measurement cross-sections for the WMS measurements were located at L=51mm, 71mm, 91mm, 111mm, 151mm, 191mm, 231mm, 271mm and L=311mm downstream of the T-junction. It is also possible to install a wire-mesh sensor on the branch side of the T-junction. Details of the WMS measurement technique can be found in [13], [14] and [18].

1.2. Selected CFD Validation Testcase, Test Geometry, Meshes

Several experiments have been carried out at ETHZ by varying the flow rates in the main and branch pipe, by exchanging the injection of tap water and de-ionized water and by changing the location of the WMSs. For the validation of the ANSYS CFX 11.0 code the test No. 14 has been selected. Main parameters of testcase No. 14 are given in Table 1.

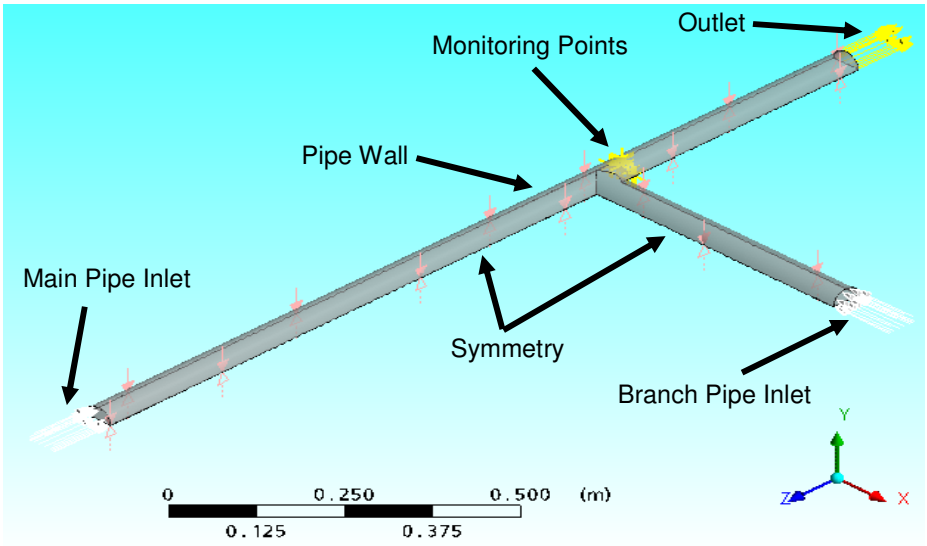

Figure 2: Geometry and boundary conditions for the ETHZ T-junction testcase.

Mesh	Nodes	Refinement Factor	Max y+	Max Angle	Min Angle	Max. Volume Change
Coarse	447 401		22	144°	41°	1.74
Medium	1 767 491	3.95	7	135°	44.5°	2.0
Fine	7 830 664	4.43	4.5	141°	40.9°	2.08

Table 2: Main parameters of mesh hierarchy for the ETHZ T-junction testcase geometry.

Since the selected testcase is isothermal, so with equal water temperature in both the main and branch pipes, the mixing of the water from both pipes characterized by the water quality can be tackled by means of Reynolds-averaged Navier-Stokes equations (RANS). The geometry of the investigated testcase is shown in Fig. 2, where advantage is taken from the inherent axial symmetry of the setup wrt. to the symmetry plane of both pipes. Therefore simulations were carried out for only one half of the geometry, which is possible in case of isothermal steady-state flow simulation, where buoyancy effects are neglected. The inlet length in front of the T-junction was L=1.0m (20D) for the main pipe and L=0.5m (10D) for the branch pipe.

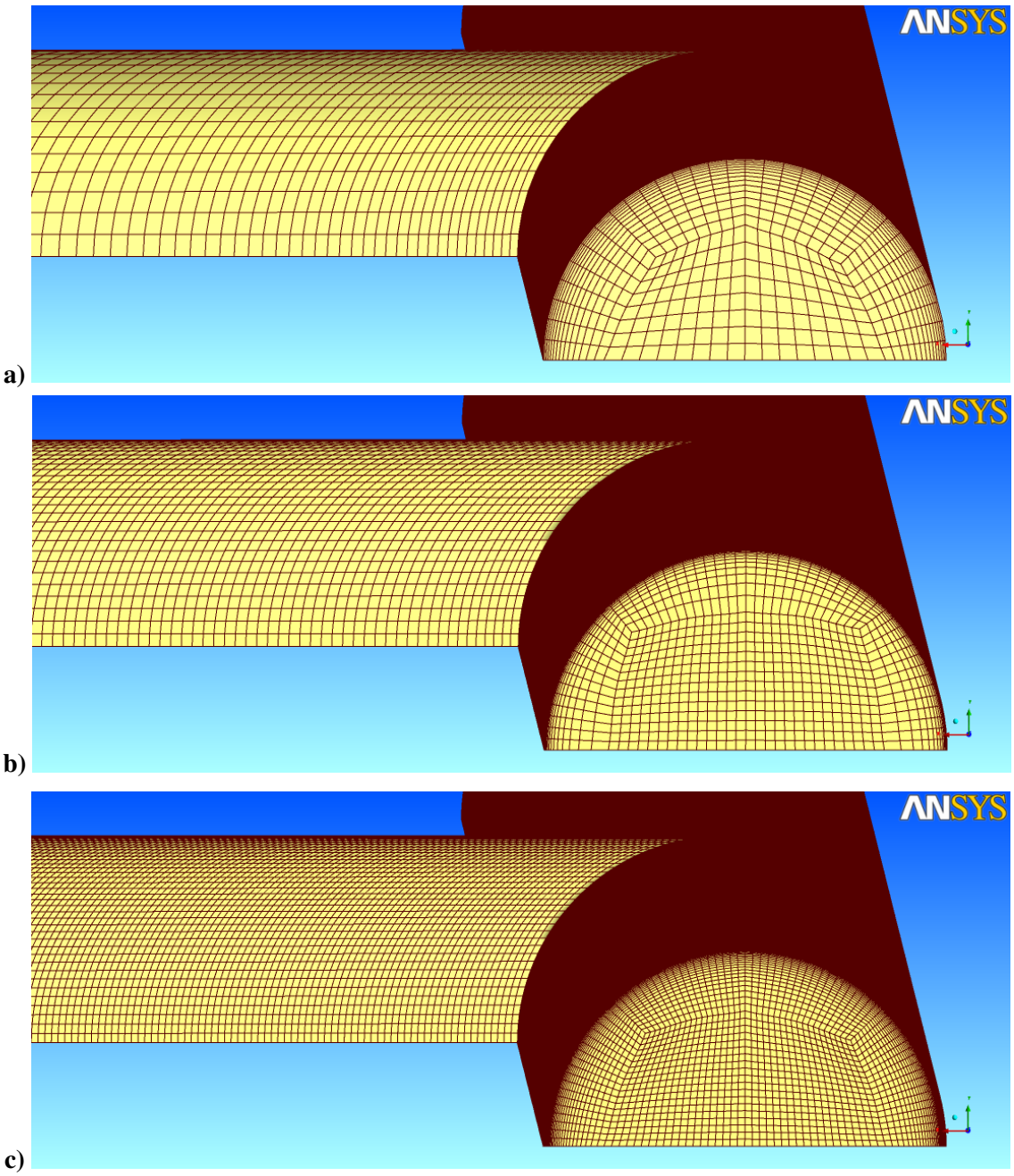

Figure 3: Hierarchy of refined meshes for the ETHZ T-junction testcase geometry.

In order to characterize numerical and modeling errors in accordance with the Best Practice Guidelines (BPG) [9], a hierarchy of 3 differently refined meshes has been generated, using the ANSYS ICEM-CFD Hexa mesh generator. Main characteristics of the hierarchical grids are given in Table 2. Figures showing the cross-sectional mesh refinement and the mesh resolution of the branch pipe can be seen in Fig. 3a)-c) for the coarse, medium and fine mesh. Quality of the meshes has been carefully maintained for all three mesh levels, as documented by the min. and max. mesh angles and the max. volume change for mesh elements.

1.3. CFD Simulation Setup and Boundary Conditions

The simulations on all three meshes were carried out using steady-state RANS simulation with the Shear Stress Transport (SST) turbulence model [8]. The SST model applies a k-ω based model formulation in proximity of the wall and the k-ε model in the bulk of the flow, while a blending function ensures a smooth transition between the two models. Automatic wall functions were used, where a maximum y^+=4.5 on the finest mesh assures, that the boundary layer can be fairly well resolved on this fine mesh. Since the flow in the T-junction is highly anisotropic where both flow streams mix and downstream of the T-junction, further studies have been carried out by applying the k-ω based Baseline Reynolds Stress Model (BSL-RSM) [2].
The concentration of the de-ionized water has been simulated in both cases by solving a transport equation of a passive transport scalar Φ:

$$\frac{\partial}{\partial t}(\rho\Phi)+\frac{\partial}{\partial x_j}(\rho U_j\Phi)=\frac{\partial}{\partial x_j}\left(\Gamma_{eff}\frac{\partial\Phi}{\partial x_j}\right)+S_\Phi \tag{1}$$

where:

$$\Gamma_{eff}=\rho D_\Phi+\frac{\mu_t}{Sc_t} \tag{2}$$

and D_Φ is the kinematic diffusivity, S_Φ is a source term for Φ (equal to zero in the present case) and Sc_t is the turbulent Schmidt number. The later term arises from the application of the eddy viscosity hypotheses in the Reynolds averaging process of this transport equation. Usually it is assumed, that the turbulent Schmidt number Sc_t~0.9. But it is known from literature, that other values have to be applied, e.g. for free jet flows in order to achieve numerical simulation results in close agreement to experiments. Therefore in the present study the turbulent Schmidt number was varied in the range $0.1 \leq Sc_t \leq 0.9$.

L=51mm

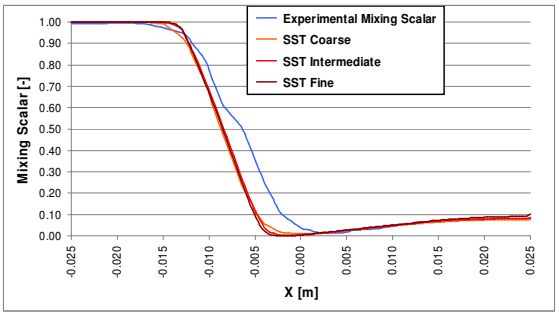

L=191mm

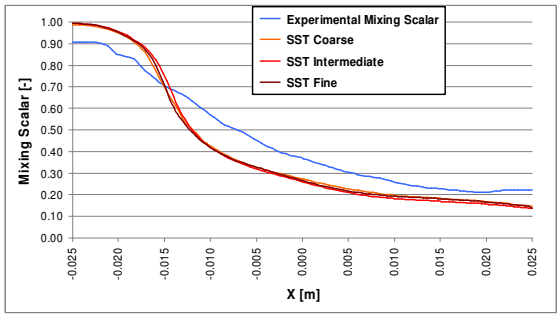

Figure 4: Profiles of the mixing scalar at two locations downstream of the T-junction for SST turbulence model simulations on 3 different meshes.

In the simulations 1/6 power law velocity profiles in accordance with the specified mean water velocity of 0.5m/s in both main and branch pipes have been specified. The given inlet length of more then 10D allows for a fairly well developed turbulent velocity profile at the mixing point of both water streams in the T-junction. In addition a medium turbulence intensity level of 5% is specified at each inlet. For the mixing scalar Φ a value of 0.0 was set at the branch pipe inlet and 1.0 for the main pipe. For the outlet a zero average static pressure outlet boundary condition has been applied. No slip conditions are set at the walls and a symmetry boundary condition has been assumed for the central symmetry plane of the geometry (see Fig. 2).

1.4. CFD Simulations and Comparison to WMS Measurements

First of all sensitivity studies with the SST turbulence model and the default value of Sc_t=0.9 have been carried on all three different mesh levels for varying characteristic timescales of the false timestep integration of ANSYS CFX, which is used as a means of underrelaxing the equations as they iterate towards the final solution. Because the solver formulation is robust and fully implicit, a relatively large time scale can typically be selected, so that the convergence to steady-state is as fast as possible. No sensitivity of the numerical algorithm was found with respect to the characteristic timescale, which was set to Δt=1.0s. The convergence criterion was set to 10^{-5} for the maximum residuals, which could be obtained in all simulation runs. Furthermore the mesh sensitivity was found to be not very large as well, as can be seen in Fig. 4 from the comparison of profiles of the mixing scalar at L=51mm and L=191mm behind the T-junction for an SST turbulence model simulation with Sc_t=0.2. Coarse and medium mesh results differ only slightly in location of large gradient of the mixing scalar, so that the fine mesh results can be regarded as mesh independent solutions.

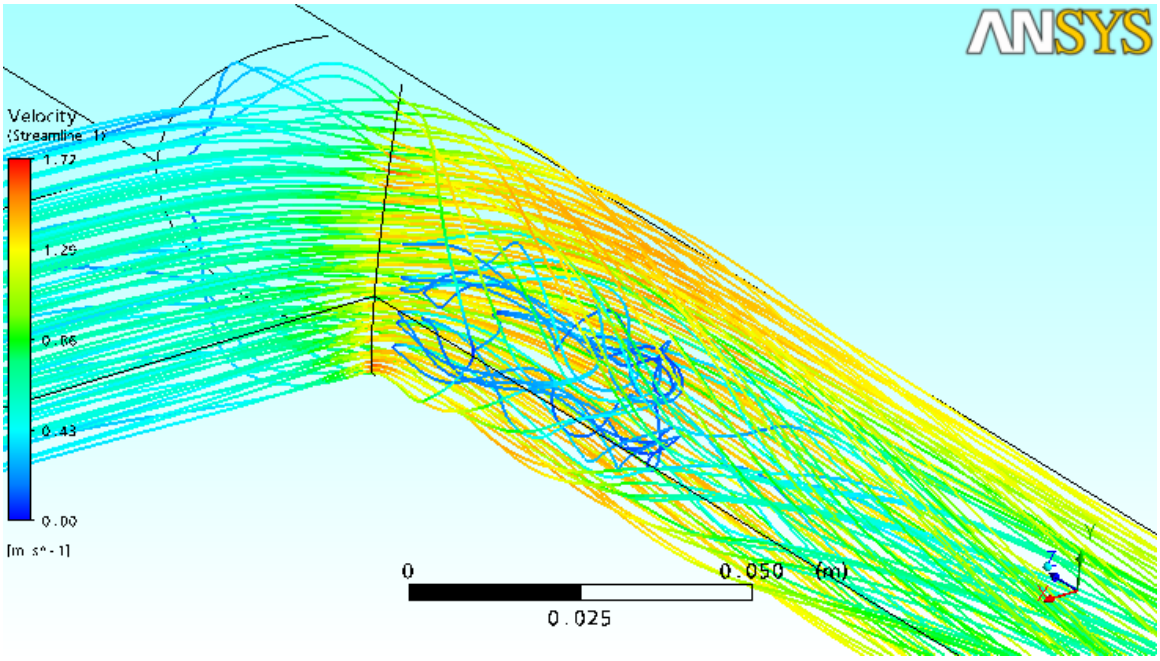

Figure 5: Streamlines of the turbulent mixing behind the T-junction. Double vortex system is developing on the inner pipe wall behind the T-junction.

For the comparison of the established CFD results with the 16×16 wires WMS measurements the experimental data were read into the ANSYS CFX solver and were assigned to a so-called additional variable. By that means the experimental data are available for any kind of post-processing in ANSYS CFX-Post, also it has to be kept in mind, that the spatial resolution of the WMS data is limited and restricted to the area between the first and last measurement cross-section.

During sensitivity analysis with respect to turbulent Schmidt number in the mixing scalar transport equation (1.1) it was found, that the default value of Sc_t=0.9 resulted in substantially to large gradients of the mixing scalar, i.e. a too sharp separation of the water stream of high and low mixing scalar values and a substantially underpredicted mixing of the two fluids. This result was established almost independently from the applied turbulence model and occurred in the CFD results for the SST and BSL RSM turbulence model as well.

L=51mm, SST

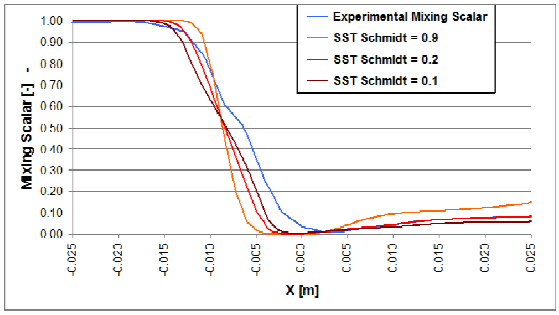

L=51mm, BSL RSM

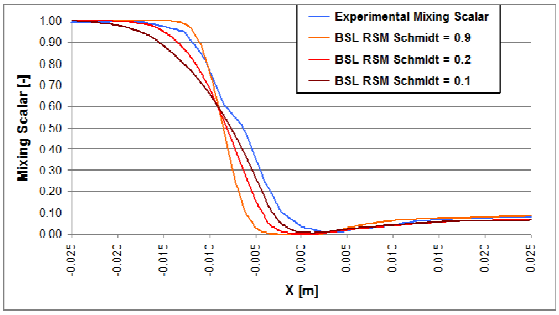

L=91mm, SST

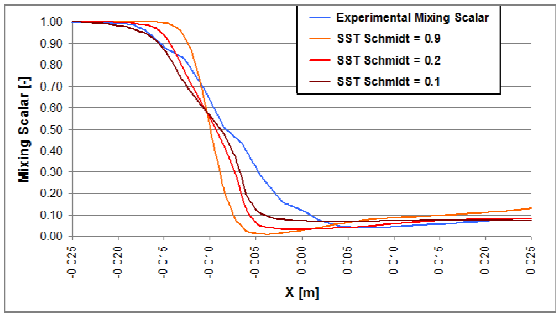

L=91mm, BSL RSM

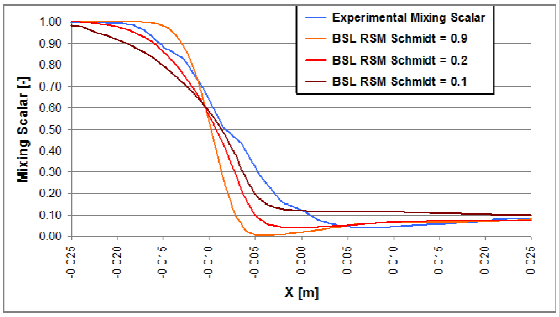

L=191mm, SST

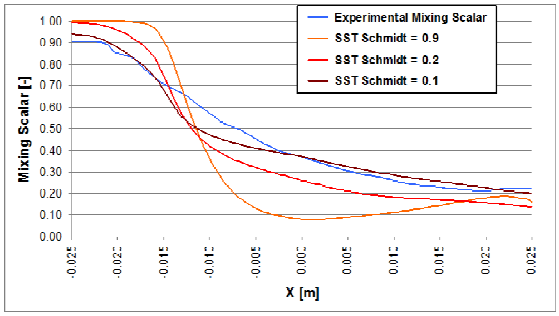

L=191mm, BSL RSM

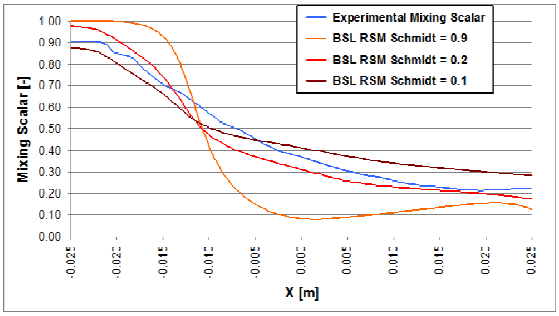

L=311mm, SST

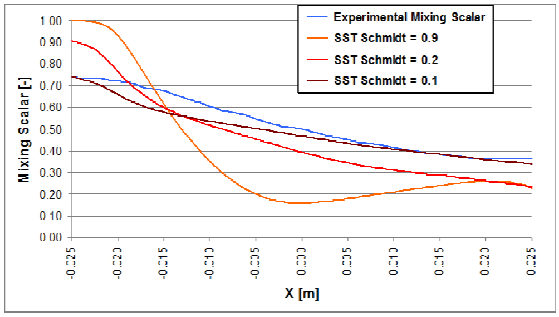

L=311mm, BSL RSM

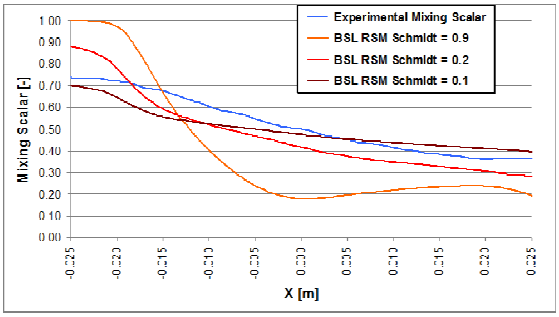

Figure 6: Profiles of the mixing scalar for 4 different distances downstream of the T-junction for SST and BSL RSM turbulence model and different Sc_t values.

L=51mm

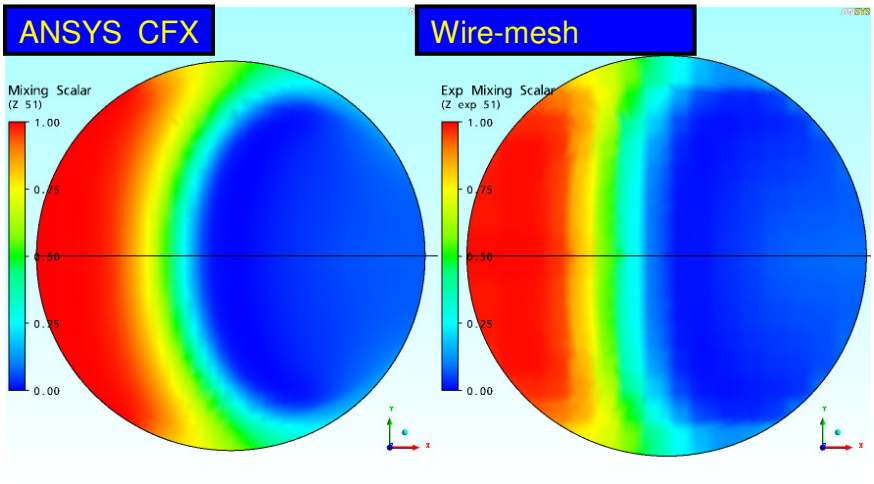

L=111mm

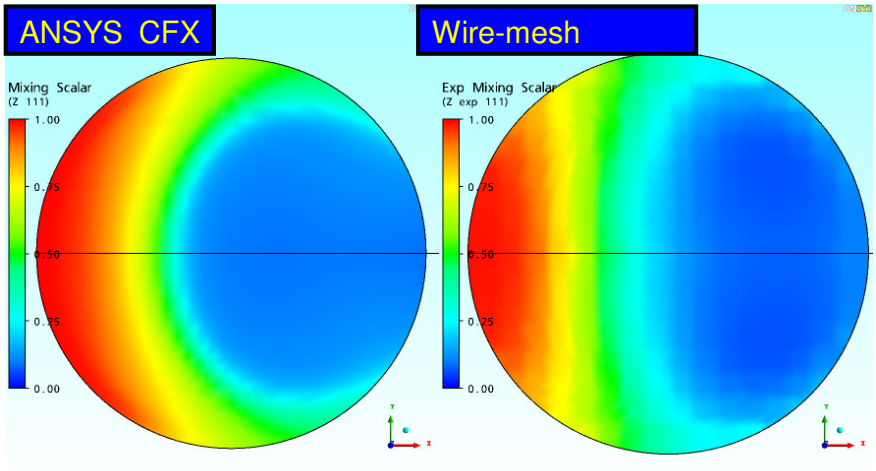

L=191mm

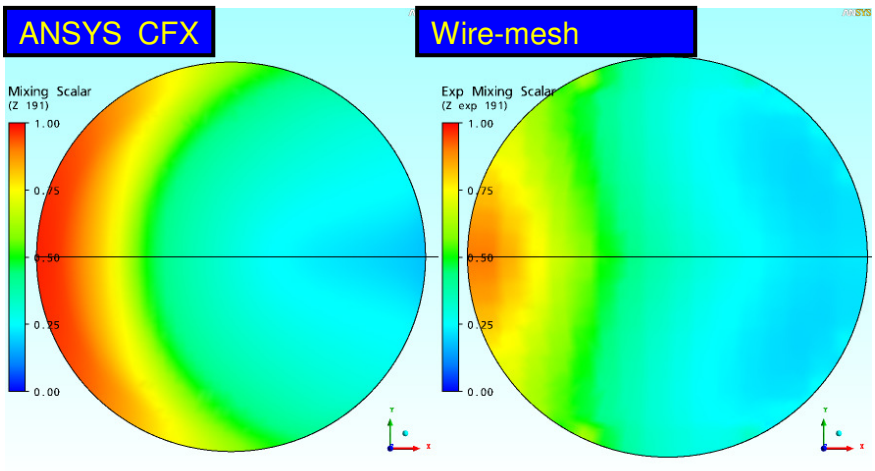

Figure 7: Cross-sectional distribution of the mixing scalar: BSL RSM turbulence model predictions (Sc_t=0.2) vs. WMS measurements.

By variation of the turbulent Schmidt number best agreement with the WMS measurements could be obtained for the investigated testcase for Sc_t=0.2. Fig. 6 shows corresponding comparison of parameter variation study using Sc_t=0.9, 0.2 and 0.1 for SST and BSL RSM turbulence model simulations in comparison to the experimental data at L=51mm, L=91mm, L=191mm and L=311mm downstream of the T-junction. Results obtained by using the BSL RSM turbulence model are generally in slightly better agreement with the experimental data. But the established increase in simulation accuracy for the mixing process seems not to be in a good relationship to the substantially higher computational effort for the higher-order turbulence model.
Finally Fig. 7 shows representative cross-sectional plots of the mixing scalar distribution for the measurement cross-sections at L=51mm and L=191mm downstream of the T-junction. Pictures show, that the high mixing scalar concentration is transported by the forming and counter-rotating double-vortex behind the T-junction along the lower and upper pipe walls, while low values of the mixing scalar (indicating water from the branch pipe) remains for quite a long distance behind the T-junction at the right side of the main pipe, where the vortex cores induced by the branch pipe flow are located. Looking at figures for L=191mm it seems that the mixing process is despite the used Sc_t=0.2 still slightly faster in the experiment where the high mixing scalar concentration values at the left side of the main pipe are already more dissolved then in the CFD simulation.

2. Vattenfall Testcase – Thermal Striping in Thermal Fluid Mixing

In contrary to the turbulent mixing of two fluid streams of equal temperature, which can obviously quite accurately be described by traditional RANS models, the thermal mixing of two fluid streams of different temperature is a rather challenging testcase for Computational Fluid Dynamics (CFD). The CFD methods based on RANS, which are typically used in industrial applications, have difficulties to provide accurate results for this flow situation. In many cases the high turbulent viscosity predicted from the RANS based turbulence models in the mixing zone due to the locally high shear rates suppress any transient flow development and the CFD results tend to a steady-state solution. On the other hand side experimental observations clearly state strong and high-frequency temperature transients at pipe walls downstream of the T-junction, the so-called thermal striping effect, which can lead to high-cycle thermal fatigue, crack formation and pipeline break in practical applications, e.g. in pipelines in power plants. Recent studies using advanced scale-resolving methods such as LES and DES have shown promising results ([3], [5], [6], [7], [12], [15] and [17]). However, detailed validation of the tools and methods is still required in order to determine their range of validity and their expected accuracy.

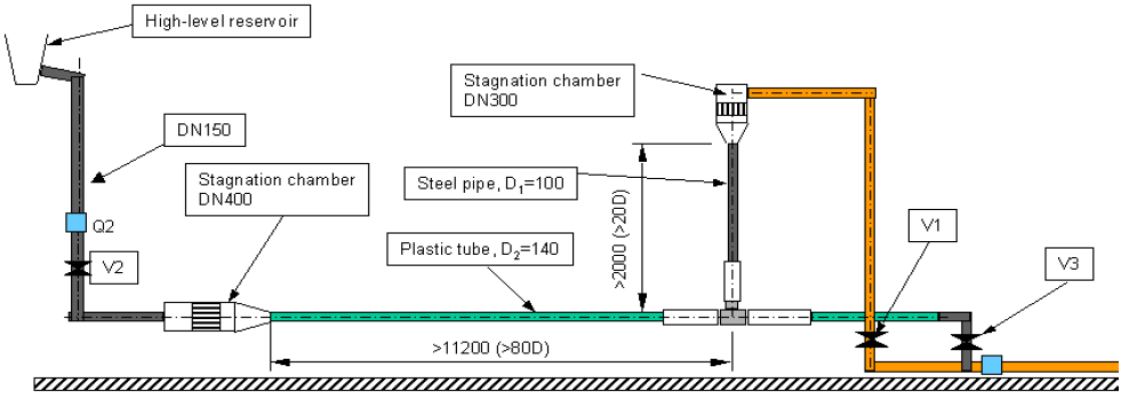

Figure 8: Side view of the Vattenfall T-junction test facility in the vertical plane (dimensions are given in mm).

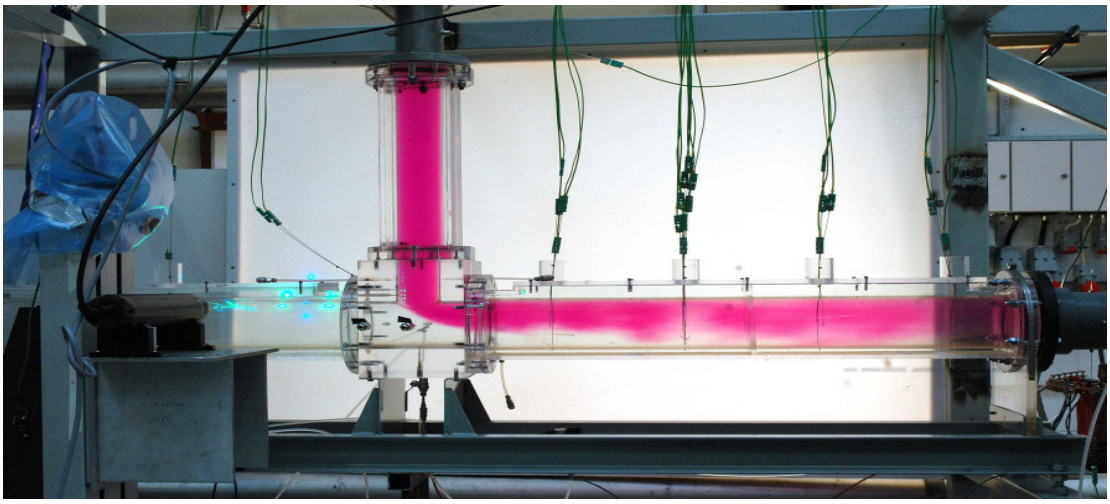

Figure 9: Side view of flow visualization test in the Vattenfall T-junction test facility.

2.1. Vattenfall T-Junction Test Facility

The model tests were carried out during 2006 at the Älvkarleby Laboratory, Vattenfall Research and Development. The related testcase conditions have been documented and provided for CFD model validation by J. Westin et al., Vattenfall [16]. The test rig is illustrated in Figures 8 and 9, and was designed in order to obtain simple and well-defined inlet boundary conditions. The setup consists of a horizontal pipe with inner diameter 140 mm for the cold water flow (Q2), and a vertically oriented pipe with inner diameter 100 mm for the hot water flow (Q1). The hot water pipe is attached to the upper side of the horizontal cold water pipe. The length of the straight pipes upstream of the T-junction is more than 80 diameters for the cold water inlet, and approximately 20 diameters for the hot water inlet. A stagnation chamber with flow improving devices (tube bundles and perforated plates) is located at the entrance to each of the two inlet pipes. The origin of the coordinate system is in the centre of the T-junction.

The temperature fluctuations near the walls were measured by Westin et al. [1], [16] with thermocouples located approximately 1 mm from the pipe wall. Two different types of thermocouples were used, with an estimated frequency response of 30 Hz and 45 Hz respectively. Velocity profiles were measured with two-component Laser Doppler Velocimetry (LDV) in each inlet pipe as well as in cross-sections located 2.6 and 6.6 diameters downstream of the T-junction. The mixing process has also been studied with single-point Laser Induced Fluorescence (LIF) at isothermal conditions. The pipes near the T-junction were made of plexiglass tubes surrounded by rectangular boxes filled with water in order to reduce the diffraction when the laser beams pass the curved pipe walls.

The tests were carried out with a constant flow ratio Q2/Q1=2, which implies approximately equal flow velocities in the two inlet pipes. The temperature difference between the hot and cold water was 15°C (hot water temperature T1=30°C), and the Reynolds number in both inlet pipes were approximately $1.9 \cdot 10^5$ for the test case considered in the present paper with bulk velocities of approximately 1.53 m/s in the hot leg and 1.56 m/s in the cold leg (corresponding to Q1=12 l/s and Q2=24 l/s). Tests were also carried out [1] with the same flow ratio but varying Reynolds number ($0.5 \cdot 10^5$ and $1 \cdot 10^5$) showing similar results.

As mentioned earlier for the provided testcase it was applied significant care to establish well-defined inlet boundary conditions for CFD model validation tests. The LDV-measurements in the cold water pipe just upstream of the T-junction showed mean velocity and turbulence profiles in good agreement with experimental data on fully developed pipe flow at similar Reynolds numbers. The length of the hot water inlet pipe was too short (20 diameters) to obtain fully

developed flow conditions, but the inlet velocity profiles were measured in order to obtain inlet boundary conditions for the simulations. Therefore for the following CFD investigations the measured velocity profiles were used for both inlet cross-sections.
When comparing computational and experimental results for the observed temperature fields non-dimensional quantities are compared, such as

$$T^* = \frac{T - T_{cold}}{T_{hot} - T_{cold}} \tag{3}$$

The normalization reduces the influence of small temperature variations between different test days. In the results part of the present paper the mean temperatures near the pipe walls are reported at the left, right, top and bottom side of the pipe. Due to a mistake when assembling the T-junction, the thermocouples in cross sections z=2D, 4D, 6D and 8D are rotated 4° as compared to the design specifications, which must be taken into account when interpreting the data.

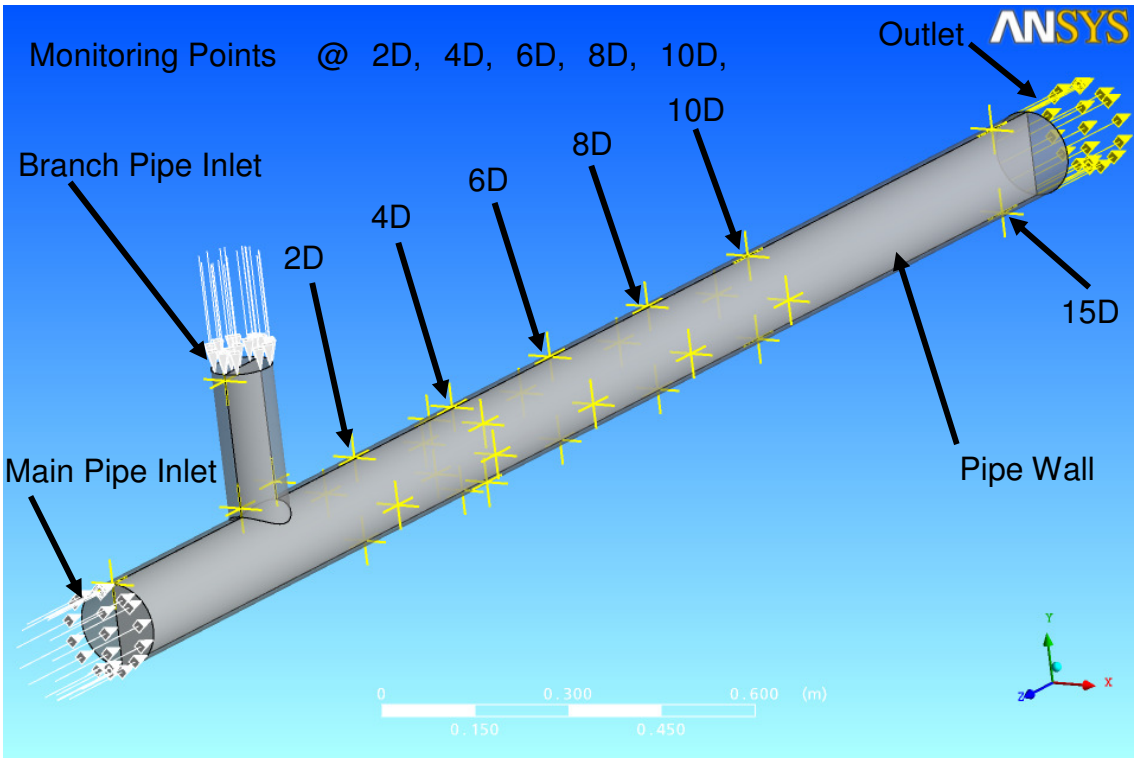

Figure 10: Geometry and boundary conditions for the Vattenfall T-junction testcase.

Flow rate in branch pipe (Q1, hot water)	12 [l/s]
Flow rate in main pipe (Q2, cold water)	24 [l/s]
Mean bulk velocity in branch pipe	1.53 [m/s]
Mean bulk velocity in branch pipe	1.56 [m/s]
Reynolds number for hot leg	$1.9 \cdot 10^5$
Reynolds number for cold leg	$1.9 \cdot 10^5$
Hot water temperature	30.0 [°C]
Cold water temperature	15.0 [°C]

Table 3: Main parameters of the thermal mixing Vattenfall T-junction testcase.

a)

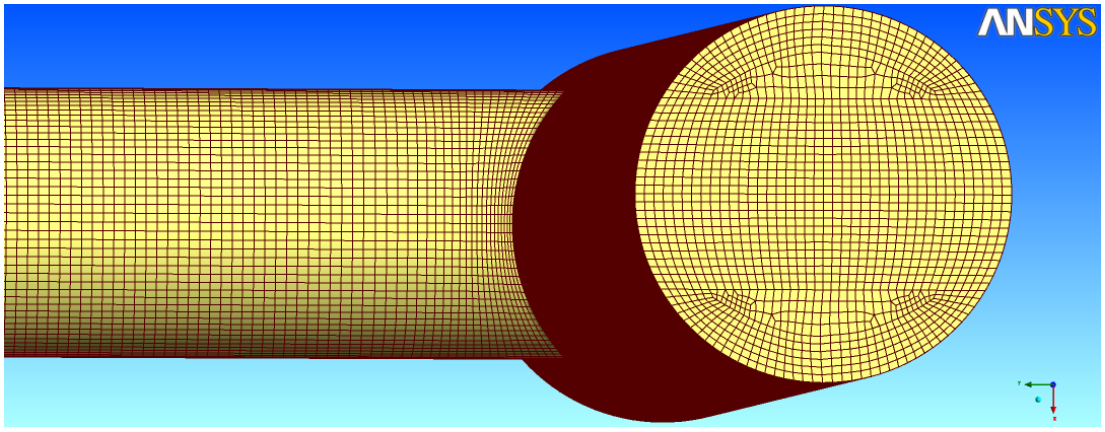

b)

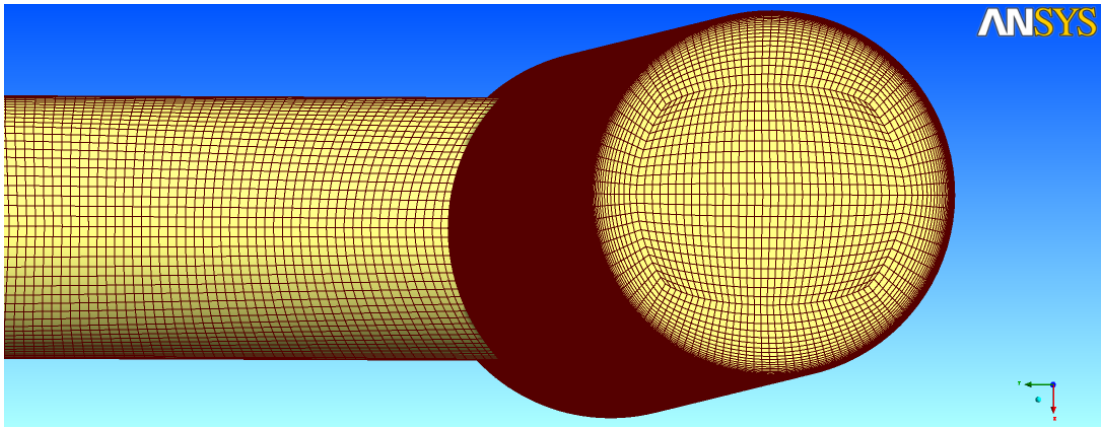

Figure 11: Hexahedral meshes generated for the Vattenfall T-junction testcase geometry.

2.2. Selected CFD Validation Testcase, Test Geometry, Meshes

From the three different experiments as provided in [16] for the validation investigation the so-called "200%" testcase has been selected, referring to the Reynolds numbers, mean bulk velocities and volume flow rates as given in section 2.1. Main parameters of the testcase are given in Table 3.

Mesh	Nodes	Refinement Factor	Max y [mm]	Max y+
Mesh 1	968.209		3.34	680
Mesh 2	2.256.320	2.33	0.1	33.2

Table 4: Main parameters of mesh hierarchy for the Vattenfall T-junction testcase geometry.

Since it is well known from literature, that the thermal striping phenomena can not be accurately predicted by RANS or URANS based simulation approaches, the goal of the current investigation was the application of scale-resolving turbulence modeling to the testcase. For this purpose a high spatial and temporal resolution of the flow is necessary, which assures CFL numbers in the order of 1 everywhere in the geometry, where dominating turbulent length and time scales have to be resolved. Two hexahedral meshes were generated for the geometry of the Vattenfall testcase (see Fig. 11), starting with a rather coarse grid (ANSYS TGrid) and finally coming up with a mesh showing reasonably good near wall refinement with about 2.2 Mill. mesh nodes (ANSYS ICEM-CFD Hexa). Meshes were generated scalable with minimum mesh angles of about 35 degree. The maximum y^+ values of about 33.2 on the finer mesh is comparable to the near wall mesh

refinement of the coarse mesh obtained for the ETHZ testcase, which is mainly due to the required higher homogeneity of mesh elements for the LES-like computations. Unfortunately the results on mesh 2 could not be obtained right in time for comparison in this paper, so further discussion of CFD results refer to the results as obtained for the mesh 1.
It is worth mentioning, that unfortunately the orientation of the geometry in the CFD model was not the same as for the experiment, also the origin of the coordinate system has been placed in the center of the T-junction as well. Further on we will refer to the coordinate system used in the CFD simulations, showing its z-axis directed along the axis of the main pipe and its y-axis along the centerline of the branch pipe. Accordingly velocity components u, v and w are referring to these coordinate axes as well.

2.3. CFD Simulation Setup and Boundary Conditions

For the CFD investigation the inlet geometry was shortened to the locations of the LDV measurements in the cross-sections in the main and branch pipe in front of the T-junction (see Fig. 10), since exactly the measured mean velocity profiles from the experimental data were prescribed here as inlet boundary conditions for the CFD simulation. Therefore inlet BC's have been prescribed at the upstream cross sections at $z=-3D_2$ for the cold leg (main pipe) and at $y=-3.1D_1$ for the hot leg (branch pipe). Profiles of turbulent kinetic energy and turbulent dissipation were derived from the LDV data for both inlets. No transient inflow boundary conditions, e.g. generation of unsteady velocity fluctuations according to turbulence spectra or use of unsteady pipe flow data, has been prescribed at the inlets. As for the ETHZ testcase a zero averaged static pressure outlet BC has been used for the outlet cross-section and non-slip BC's with automatic wall treatment are used for all walls of the domain. Since the meshes were generated for the full 3d geometry there was no more need for a symmetry boundary condition. Additionally so-called monitoring points were introduced at all locations of thermo-couples, as can be seen from Fig. 10, in order to monitor the transient history of main characteristics, i.e. fluid temperature at these locations for comparison with the data.
For meshes 1 and 2 some basic investigations have been carried out for the verification of the CFD setup, the investigation of mesh independency of the CFD solution and for the quantification of the numerical error in steady-state and transient simulation using the Shear Strain Transport (SST) turbulence model in RANS and URANS mode. The temperature dependent fluid properties (density, viscosity) have been taken into account by defining the water properties from the industry standard IAPWS-IF97. Based on resulting fluid density differences fluid buoyancy has been taken into account.
For the transient URANS SST and SST-SAS simulations a second-order backward Euler time discretization with a timestep of $\Delta t=0.001s$ was used and a convergence criterion based on the maximum residuals of 10^{-4} was reached at every timestep with 3-5 coefficient loops (sub-iterations) per timestep. The high-resolution advection scheme has been applied for the spatial discretization of momentum equations. It was found, that after some initial transient behavior the URANS SST solution was quickly approaching a steady-state solution in terms of velocity and temperature fields. This result is as expected from the experience of other researchers and underlines the strong requirement for scale-resolving turbulence models for this type of applications. The solution obtained with the URANS SST model furthermore has been used as an initialization for the further transient investigations using the scale-resolving SST-SAS turbulence model.
The so-called Scale-Adaptive Simulation (SAS) model was recently proposed by Menter & Egorov [10], [11] as a new method for the simulation of unsteady turbulent flows. The formulation can operate in standard (U)RANS mode, but has the capability of resolving the turbulent spectrum in unsteady flow regions. The method is termed Scale-Adaptive Simulation (SAS) modeling, as it adapts the length-scale automatically to the resolved scales of the flow field. The distinguishing factor in the model is the use of the von Karman length-scale, L_{vK}, which is a

three-dimensional generalization of the classic boundary layer definition $\kappa U'(y)/U''(y)$ (for details see [4]). The governing equations of the SST-SAS model differ from those of the SST RANS model by the additional SAS source term Q_{SAS} in the transport equation for the turbulence eddy frequency ω:

$$\frac{\partial \rho k}{\partial t} + \nabla \bullet (\rho \mathbf{U} k) = P_k - \rho c_\mu k \omega + \nabla \bullet \left[\left(\mu + \frac{\mu_t}{\sigma_k} \right) \nabla k \right] \tag{4}$$

$$\frac{\partial \rho \omega}{\partial t} + \nabla \bullet (\rho \mathbf{U} \omega) = \alpha \frac{\omega}{k} P_k - \rho \beta \omega^2 + Q_{SAS} + \nabla \bullet \left[\left(\mu + \frac{\mu_t}{\sigma_\omega} \right) \nabla \omega \right] + \\ + (1 - F_1) \frac{2\rho}{\sigma_{\omega 2}} \frac{1}{\omega} \nabla k \nabla \omega \tag{5}$$

where $\sigma_{\omega 2}$ is the σ_ω value for the k-ε regime of the SST model and the source term Q_{SAS} reads:

$$Q_{SAS} = \max \left[\rho \zeta_2 \kappa S^2 \left(\frac{L}{L_{vK}} \right)^2 - C \cdot \frac{2\rho k}{\sigma_\Phi} \max \left(\frac{|\nabla \omega|^2}{\omega^2}, \frac{|\nabla k|^2}{k^2} \right), 0 \right] \tag{6}$$

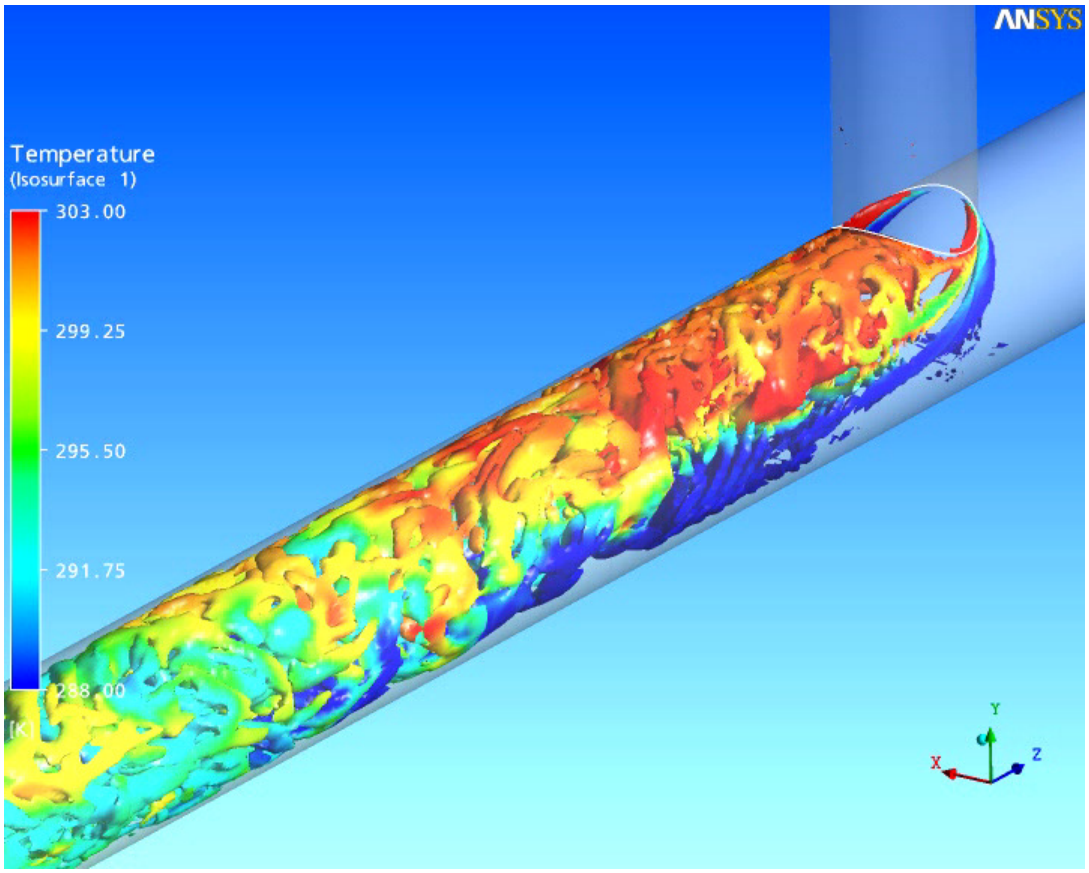

Figure 12: Vortex structure developing downstream of the Vattenfall testcase T-junction as visualized by isosurfaces of the Q criteria (mesh 1, Q=100 $1/s^2$).

a) z=2D, time averaged velocity $\sqrt{\overline{u}^2+\overline{v}^2}$

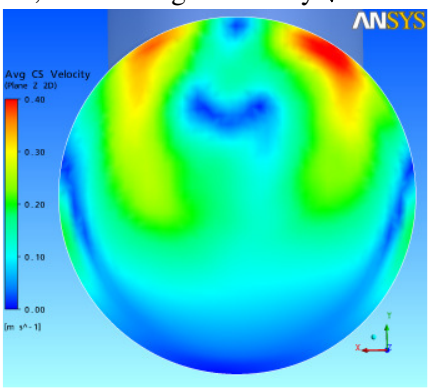

b) z=6D, time averaged velocity $\sqrt{\overline{u}^2+\overline{v}^2}$

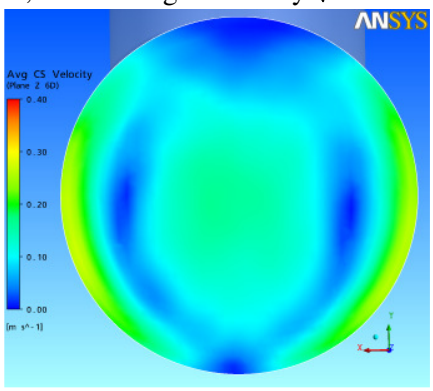

c) z=2D, time averaged temperature

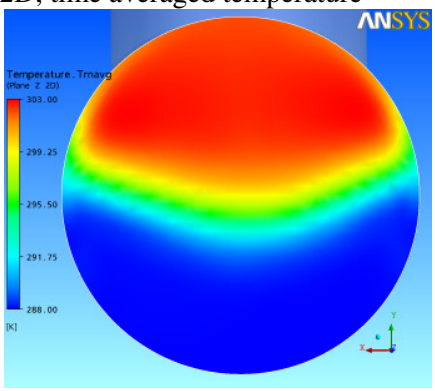

d) z=6D, time averaged temperature

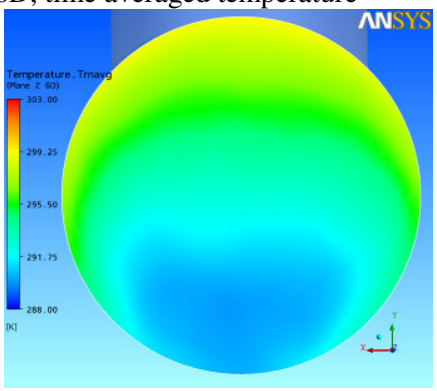

e) x=0, time averaged velocity

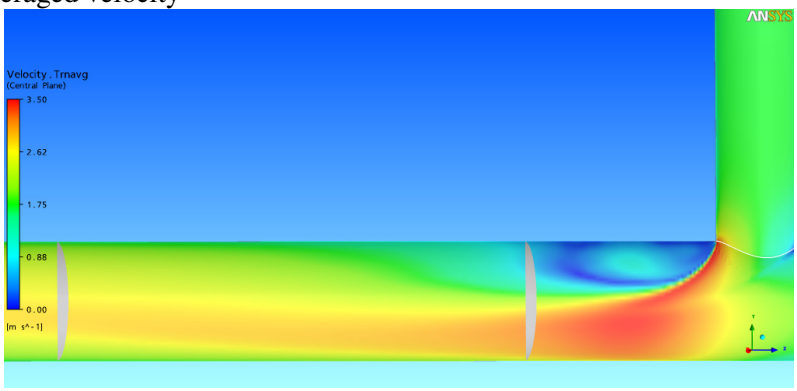

f) x=0, time averaged temperature

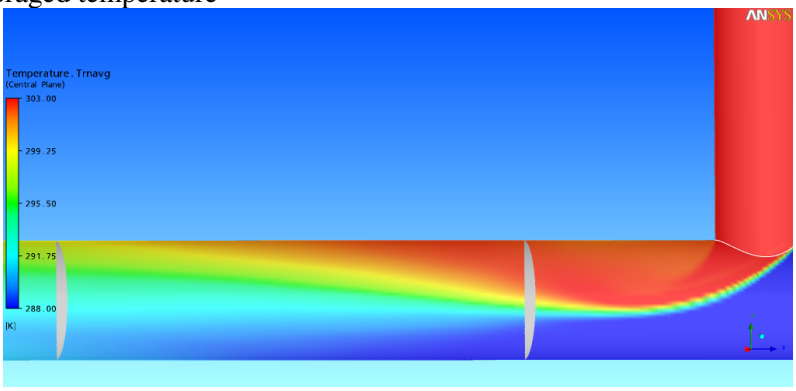

Figure 13: Time averaged velocity and temperature distributions.

A complete description of the SST-SAS model can be found in the publications [4] and [11]. Contrary to standard URANS models, the SAS formulation provides a turbulent length-scale, which is not proportional to the thickness of the turbulent (shear) layer, but proportional to the local flow structure. The SAS solution automatically applies the RANS mode in the attached boundary layers, but allows a resolution of the turbulent structures in the detached regime. This behavior is in much better agreement with the true physics of the flow, as was also shown for other cases by Menter and Egorov [4], [10], [11]. The "LES"-like capability of the model is achieved without an explicit dependency on the grid spacing, contrary to classical LES methods.

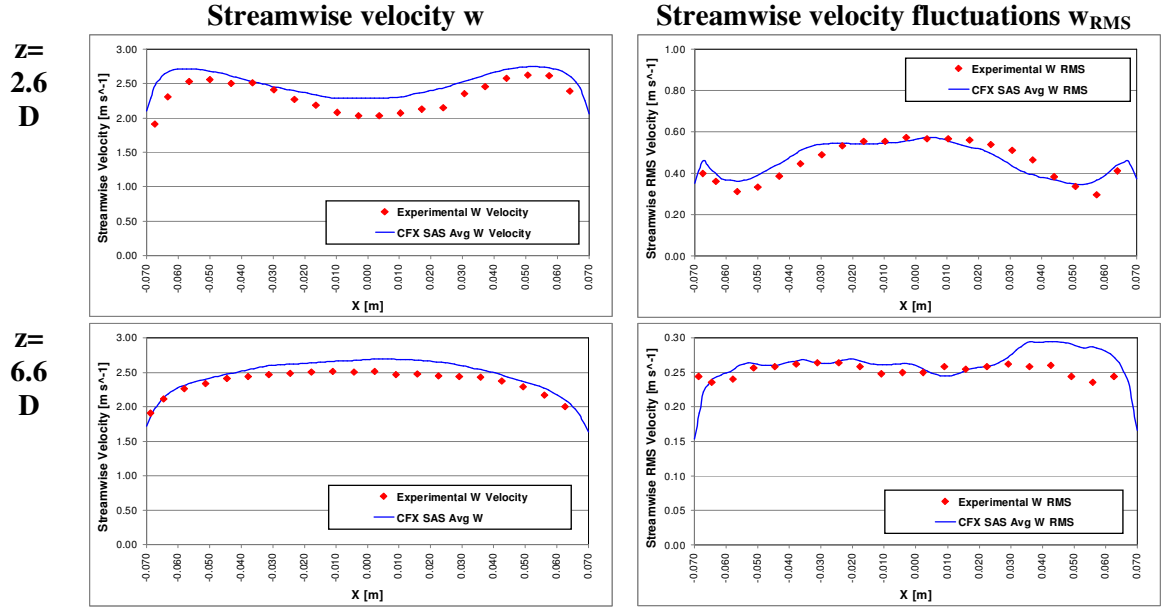

Figure 14: Time averaged streamwise w velocity and w velocity fluctuations at y=0; z=2.6D and z=6.6D.

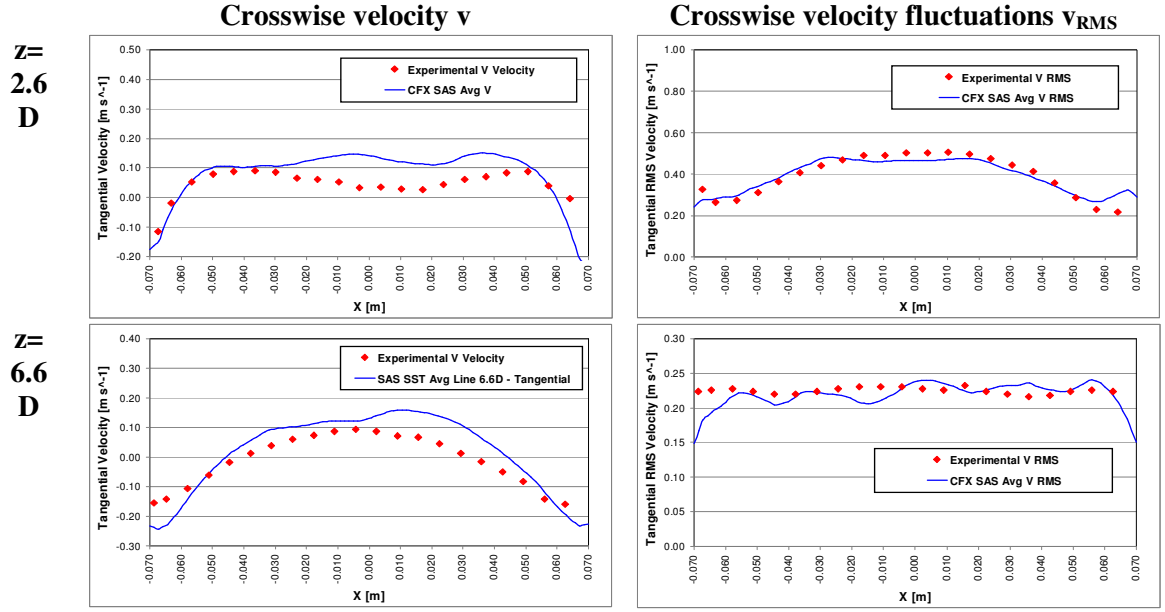

Figure 15: Time averaged crosswise v velocity and v velocity fluctuations at y=0; z=2.6D and z=6.6D.

2.4. CFD Simulations and Comparison to Data

As already mentioned, the SAS-SST solution on the meshes 1 and 2 for the Vattenfall testcase geometry was initialized at T=0.0s with the quasi steady-state result from the preceding SST URANS simulation on the same mesh. Then transient simulation by using the SAS-SST scale-resolving turbulence model approach has been carried out for 7.6s real time with a time step of Δt=0.001s, where after a first 1.48s the transient averaging of mean flow field characteristics (e.g. mean velocity and temperature) has been started.

Fig. 12 shows the typical developing vortex structures downstream of the T-junction at T=7.6s real time. The visualization is based on isosurfaces of the so-called Q-criteria, where:

$$Q = \Omega^2 - S^2 = \left(\frac{\partial u_i}{\partial x_j} - \frac{\partial u_j}{\partial x_i} \right)^2 - \left(\frac{\partial u_i}{\partial x_j} + \frac{\partial u_j}{\partial x_i} \right)^2 \tag{7}$$

with Ω being the vorticity and S the strain rate of the flow field. The figure clearly shows that the small change in the Vattenfall T-junction geometry in comparison to the ETHZ testcase by choosing a smaller diameter for the branch pipe leads to the formation of a so-called horseshoe vortex upstream the intruding hot water jet from the branch pipe. Furthermore the figure shows rather irregular turbulent vortex structures forming immediately downstream of the T-junction and being convected with the flow along the main pipe. Further downstream it can be observed, that the length scale of the vortex structures decreases with turbulent dissipation.

Fig. 13 shows the time averaged velocity and temperature distributions in cross-sections at z=2D, z=6D and x=0. Mean temperature distribution in Fig. 13c) still shows for z=2D a rather sharp stratification of the hot and cold fluid with cold fluid temperature at the locations of thermocouples at the side walls of the pipe (in the statistically averaged temperature field). In the cross section at z=6D in Fig. 13d) the enhanced turbulent mixing has led to a propagation of high temperature liquid along the pipe walls, where rather high averaged fluid temperatures can now be observed at the φ=135° and φ=225° thermocouple locations. Furthermore Fig. 13f) shows the rather pronounced and progressed mixing at the cross section of z=6D, where the averaged fluid temperature is well below the hot fluid temperature everywhere in the cross section, also it is known from the instantaneous temperature distributions that the flow behavior is strongly transient with large temperature fluctuations. Fig. 13e) shows the recirculation zone behind the intruding hot water jet, which in turn leads to a delayed mixing of hot with cold water in that region close behind the T-junction at the top of the pipe. In the result the fluid temperature at the thermocouple sensor location on top wall of the pipe at z=2D still shows rather high fluid temperature close to the branch pipe inlet temperature.

Fig. 14 shows the streamwise w velocity and w_{RMS} velocity fluctuations at y=0; z=2.6D and z=6.6D respectively in direct comparison to the LDV measurement data at these locations. Fig. 15 shows the corresponding comparison for the crosswise v velocity and v_{RMS} velocity fluctuations in the same corresponding profiles.

The streamwise w velocity in the left hand side diagrams of Fig. 14 shows reasonable well agreement with data. Further the fluctuation velocity in streamwise direction w_{RMS} is in general good agreement with the measurements as well, also the pattern of the cross-sectional profile shows some asymmetry and some larger deviations from the data points on the right side of the pipe (positive x). This could be an indication that the averaging period in the CFD simulation of about T~6.12s real time (corresponding to 6120 iterations) was still too short in order to establish statistically reliable averaged values. Similar situation can be observed for the crosswise v velocity component and its RMS fluctuation as shown in Fig. 15. For the crosswise velocity component it can be observed, that the RMS fluctuations are substantially higher then the averaged mean values.

Furthermore comparison has been made for the axial development of the centerline v_{RMS} and w_{RMS} fluctuation velocities in the range of 1.5D≤z≤7.5D in comparison to the LDV measurements as shown in Fig. 16. The predicted values from the statistical averaging of the CFD result show again a reasonable good agreement with data and the correct decay in the amplitude of the fluctuation velocities RMS over pipe length.

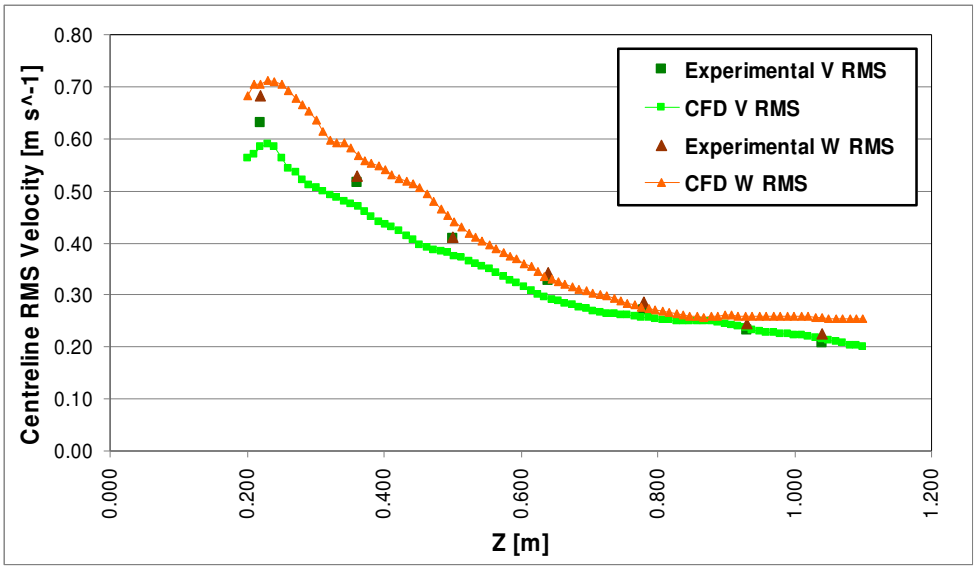

Figure 16: Development of centerline RMS velocities from z=0 to z=7.5D.

Further comparisons are made for the normalized time-averaged wall temperatures at the bottom, left and right side as well as at the top wall of the pipe at the locations of the thermocouples in the experiment (r=69mm) and comparison to their data, as shown in Figs. 17a)-d). The definition of T* corresponds to the formula as given in eq. (3). Furthermore the results of the ANSYS CFX SAS-SST model have not only compared to data, but an ANSYS Fluent simulation has been carried out on the identical mesh 1 using the SAS-SST model implementation in ANSYS Fluent. Since the mesh 1 has still a rather coarse mesh resolution in the vicinity of the pipe wall and since the different cell-centered vs. vertex-centered discretisation schemes of ANSYS CFX and ANSYS Fluent lead in that case to different locations of data representation and different resolution of the boundary layer, a second data set of temperature corresponding to a wall distance of the second mesh node at 7mm from the pipe wall (r=63mm) has been included in the diagrams.
It can be observed from Fig. 17a), that the SAS-SST simulation results agree very well with data for the thermocouple locations at the bottom wall of the pipe for the full axial range of measurements between 2≤z/D≤10. Almost no difference can be observed for the two compared numerical simulations of ANSYS CFX and ANSYS Fluent.

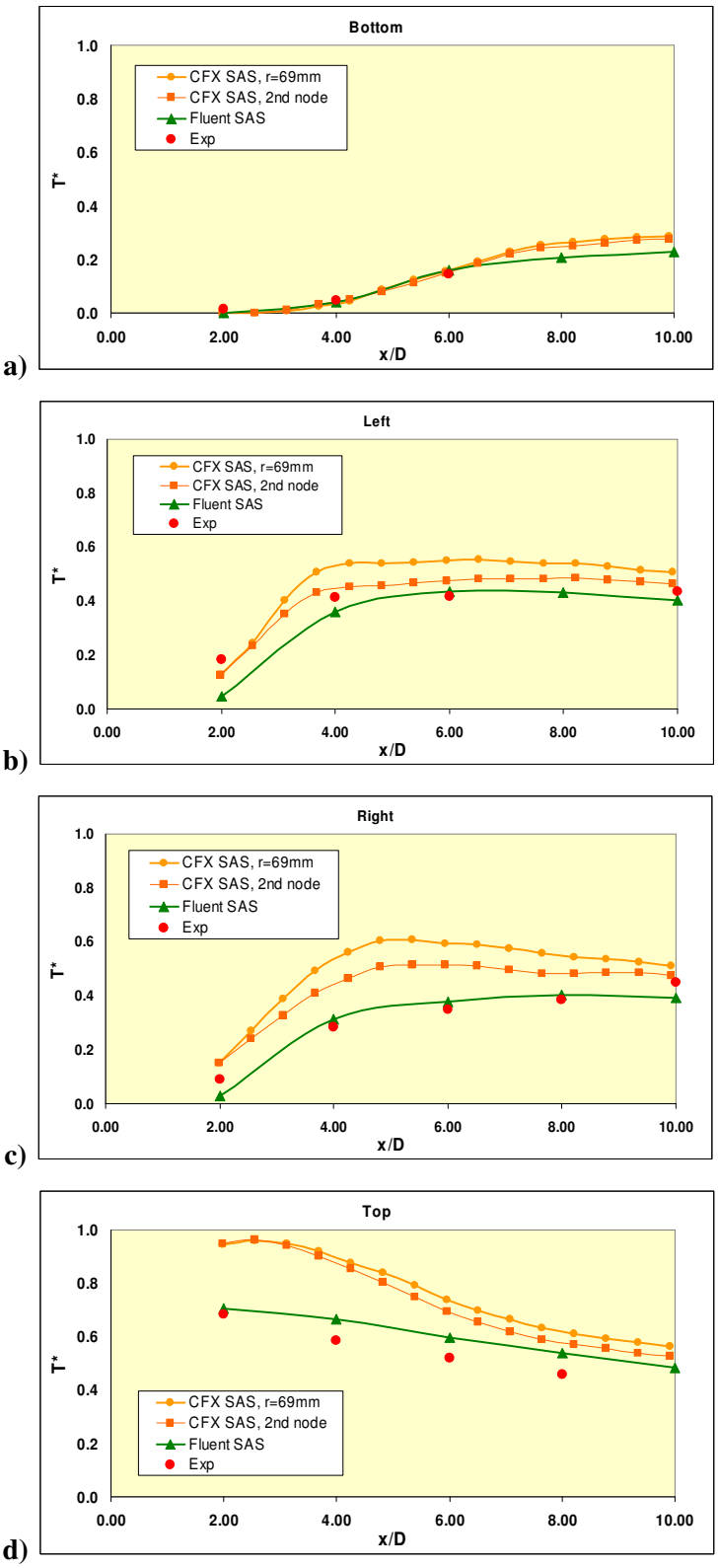

Figure 17: Development of time-averaged water temperature over pipe length for thermocouple locations at top, left and right side wall as well as at the bottom of the pipe.

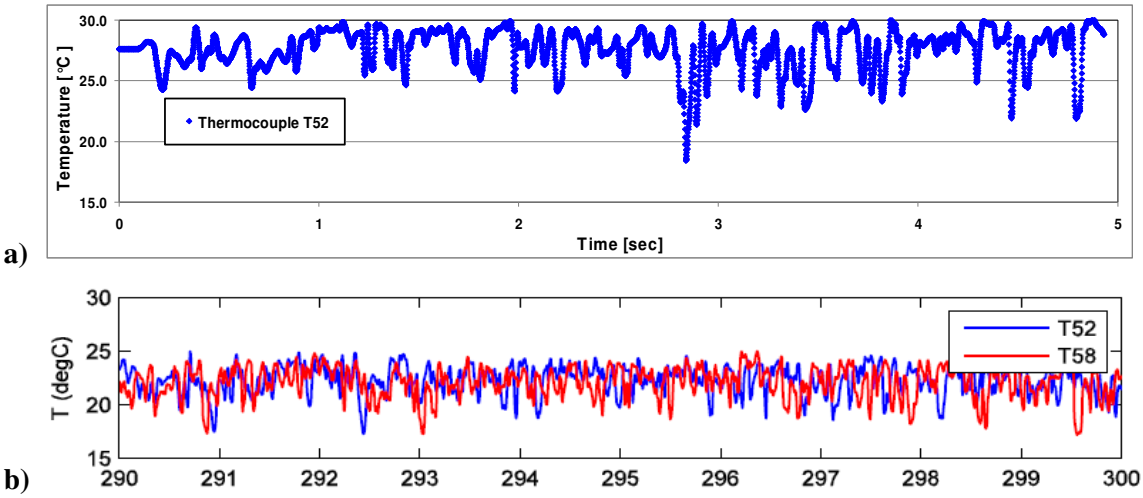

Figure 18: Temperature fluctuations over time for thermocouples T52 and T58 at z=4D; φ=±45° a): as predicted from ANSYS CFX SAS-SST simulation; b): experimental data.

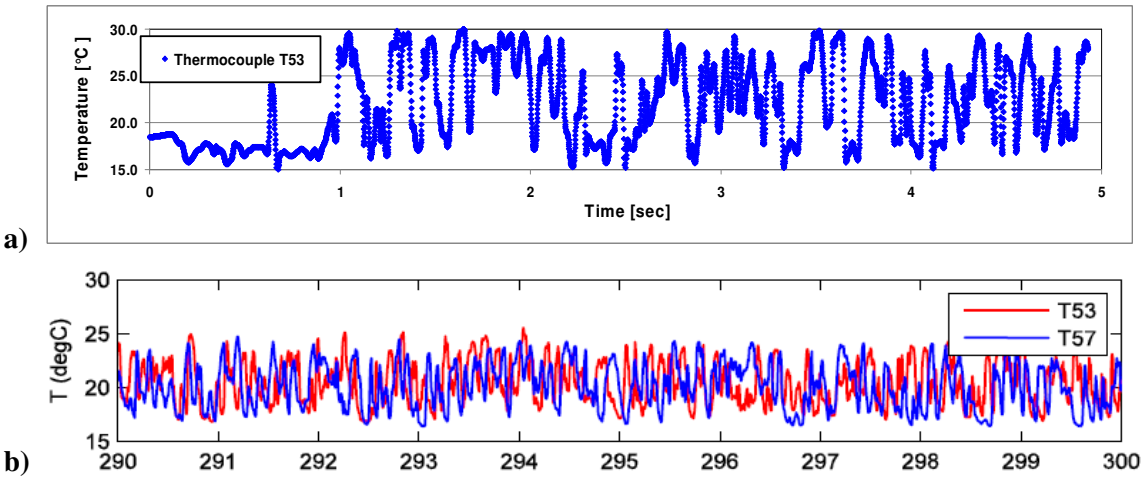

Figure 19: Temperature fluctuations over time for thermocouples T53 and T57 at z=4D; φ=±90° a): as predicted from ANSYS CFX SAS-SST simulation; b): experimental data.

In Figs. 17b) and c) the normalized time-averaged wall temperatures are compared for the left and right pipe wall locations of the thermocouples. It can be observed, that the experimental data show a slight asymmetry, especially for 2≤z/D≤6, while for obvious symmetry reasons the CFD results show almost identical values for both sides of the pipe in the long-term statistical average. It can be remarked, that the solution of ANSYS CFX delivers slightly higher temperature values in comparison to the ANSYS Fluent solution. Both are in reasonable good agreement with the thermocouple data at the left pipe wall, while the experimental temperature data at the right pipe wall are slightly lower. But it has to be taken into account and is mentioned in the experimental report [1], that it was in particular difficult throughout the different realizations of the experiment to maintain constant thermal boundary conditions, which is seen as one of the main reasons for

the requirement to normalize the measured temperature values and for possible differences to the CFD results.
Finally Fig. 17d) shows the comparison for the top wall location of thermocouples. At these locations the largest differences between the experimental data and CFD results on one hand side and between the two CFD codes on the other hand side can be observed. ANSYS CFX is predicting substantially higher fluid temperatures especially in the close distance to the T-junction, while the agreement with data becomes better with increasing pipe length, especially for z/D>6. The agreement of the ANSYS Fluent results with data for the top wall temperature sensors seems to be better over the entire range of measurement locations in comparison to the ANSYS CFX results. The reason for the observable differences are still subject of further investigations and it is expected, that the SAS-SST simulation results on mesh 2 with a better near-wall mesh refinement will provide an explanation for the discrepancy. A possible reason for the different simulation results can be found in the rather coarse near-wall mesh refinement of mesh 1 in combination with the different spatial discretisation schemes of the two CFD codes (cell-centered vs. vertex-centered discretisation), leading to a substantially different location of the wall-nearest mesh node in the boundary layer on coarse meshes and thereby to a possible different prediction of the axial extent of the recirculation zone directly behind the T-junction at the top of the pipe wall. This would substantially influence the fluid mixing at this location, providing a possible explanation for the differently predicted near-wall temperatures at the top of the pipe wall.
If we finally look on the time series of recorded thermocouple measurements in comparison to the fluid temperature recorded at the corresponding monitoring point locations, then similar patterns can be recognized. Fig. 18a) and b) show the comparison of transient temperature signals for the thermocouples T52 and T58 at z/D=4 and $\varphi=\pm 45°$ and Fig. 19a) and b) for the thermocouples T53 and T57 at z/d=4 and $\varphi=\pm 90°$. In both the CFD results and experimental data no regular frequency of the temperature fluctuation over time can be identified. As already discussed, the CFD result for the top wall of the pipe at z/D=4 (T52) shows too high mean temperature level in comparison to experiments, while the amplitude of temperature fluctuations is about ±5°C in both cases. For the side walls of the pipe at z/D=4 (T53) the amplitude of temperature fluctuations from the CFD simulation seems to be even higher then in the experiment.

3. Conclusions

Investigations have shown, that Reynolds averaging based (U)RANS turbulence models like SST or BSL RSM are able to satisfactorily predict the turbulent mixing of isothermal fluid in T-junctions, while the thermal mixing of water streams of different temperature in T-junctions is a challenging testcase for CFD methods, and advanced scale-resolving turbulence modeling approaches like LES, DES or SAS are required in order to simulate the strongly transient flow and temperature fields. The application of Best Practice Guidelines to these type of transient LES-like simulations and the thoroughly validation of the scale-resolving turbulence models today still involves a couple of unresolved questions due to the extremely high computational effort in the order of several weeks for a single transient CFD simulation.
In the present investigation two different testcases have been investigated. The turbulent mixing of water streams of equal temperature in a T-junction in the horizontal plane (ETHZ testcase) has shown to be satisfactorily predicted with steady-state computation and traditional Reynolds averaging based RANS models like SST and BSL RSM. The CFD results have been compared to the detailed wire-mesh sensor concentration measurements carried out at ETHZ test facility, by importing the WMS data into the CFD post-processor. In order to establish the very good comparison to the measurements, the turbulent Schmidt number had to be adjusted to values about 0.1-0.2 in order to reflect the strongly accelerated turbulent mixing in the pipe T-junction in this case.

The second investigated testcase was provided by Westin et al. [16] and is aimed to provide detailed experimental validation data and thoroughly prepared and monitored testcase boundary conditions for the assessment and validation of LES-like turbulence models for the further study of thermal striping phenomena occurring in thermal mixing in T-junctions. ANSYS CFX 11.0 with the scale-resolving SAS-SST approach has been applied to one of the provided testcase conditions. The CFD solutions in fact showed the occurrence of the thermal striping phenomena in the simulations. Predicted general flow patterns and time averaged mean velocity profiles are in good agreement with the experimental observations, also due to the long simulation time the averaging time (6.12s, 6120 timesteps) for the SAS simulation was probably still too short in order to establish statistically fully reliable time averaged variable fields for velocity and temperature. The predicted velocity fluctuation RMS values are in reasonable good agreement with data as well, compare reasonably well to measured profile data and show the correct reduction in RMS velocity fluctuation amplitude due to turbulent dissipation with increasing pipe length downstream of the T-junction.

Transient thermal striping was observable from the SAS-SST solution. Measured as well as predicted thermal striping patterns do not show any recognizable regular pattern in temperature fluctuations. While some differences occurred for the predicted wall temperatures at the top wall of the pipe, the predicted normalized time-averaged temperature values for the side and bottom wall thermocouple locations were in good agreement with the measurements. The onset of thermal striping for the side and bottom walls of the main pipe was predicted at about z~4D, which is in good coincidence with the observable rise in normalized time-averaged temperature from the experiments.

Application of Best Practice Guidelines to LES-like CFD simulations is still a challenge due to the extremely large computation times. Therefore special care has to be applied to the mesh generation with respect to LES criteria for resolution of turbulent length scales and with respect to the time averaging procedure in order to assure the statistical reliability of the CFD results. Further investigations are carried out in order to investigate the influence of mesh resolution on statistically averaged flow simulation results.

4. Acknowledgements

The authors like to acknowledge the good collaboration and open discussions with the team of Prof. H.-M. Prasser at ETHZ and with J. Westin at Vattenfall, who both have provided the underlying detailed and very carefully documented validation data. The author thanks F. Carlsson from ANSYS Sweden for the provision of the ANSYS Fluent simulation result for the Vattenfall testcase. Further the present investigation has been supported by the German Ministry of economy (BMWi) in the framework of the German CFD Network in Nuclear Reactor Safety.

5. References

[1] Anderson U., Westin J., Eriksson J.: “Thermal Mixing in a T-Junction. Model Tests 2006”, Report Number U 06:66, , Vattenfall R&D AB, Älvkarleby, Sweden, 2006, pp. 1-68.

[2] ANSYS CFX-11.0 User Manual, ANSYS Inc., Canonsburg, USA, November 2006.

[3] Braillard, O., Jarny, Y. and Balmigere, G.: “Thermal load determination in the mixing Tee impacted by a turbulent flow generated by two fluids at large gap of temperature”, ICONE13-50361, 13th International Conference on Nuclear Engineering, Beijing, China, May 16-20, 2005.

[4] Egorov Y., Menter F.R.: “Development and Application of SST-SAS Turbulence Model in the DESIDER Project”, Second Symposium on Hybrid RANS-LES Methods, 17/18 June 2007, Corfu, Greece, pp. 1-10.

[5] Hu L.-W., Kazimi M.S.: Large Eddy Simulation of Water Coolant Thermal Striping in a Mixing Tee Junction", The 10th Int. Topical Meeting in Nuclear Reactor Thermal Hydraulics (NURETH-10), Seoul, Korea, October 5-9, 2003, pp. 1-10.

[6] Igarashi M., Tanaka M., Kimura N., Kamide H.: "Study on Fluid Mixing Phenomena for Evaluation of Thermal Striping in a mixing Tee", The 10th Int. Topical Meeting in Nuclear Reactor Thermal Hydraulics (NURETH-10), Seoul, Korea, October 5-9, 2003, pp. 1-12.

[7] Kuszaj A.K., Komen E.: "Large-eddy simulations for thermal fatigue – An assessment on the flow characteristics", Presentation on the Meeting of the German CFD Network in Nuclear Reactor Safety, 23.-24. January 2008, Grosshartpenning, Germany, 29 slides.

[8] Menter F.R.: "Zonal Two Equation k-ω Turbulence Models for Aerodynamic Flows", AIAA Paper 93-2906, (1993).

[9] Menter F.R.: "CFD Best Practice Guidelines for CFD Code Validation for Reactor Safety Applications", EC Project ECORA, Report EVOL-ECORA-D01, pp. 1-47, 2002.

[10] Menter F. R., Egorov, Y.: "Re-visiting the turbulent scale equation", Proc. IUTAM Symposium; One hundred years of boundary layer research, Göttingen, Germany, 2004.

[11] Menter F. R., Egorov, Y.: "A scale-adaptive simulations model using two-equation models", AIAA Paper 2005-1095, 2005.

[12] Ohtsuka, M., Kawamura, T, Fukuda, T., Moriya, S., Shiina, K., Kurosaki, M., Minami, Y., Madarame, H.: "LES analysis of fluid temperature fluctuations in a mixing Tee pipe with the same diameters", ICONE 11-36064, 11th International Conference on Nuclear Engineering, Tokyo, Japan, April 20-23, 2003.

[13] Prasser, H.-M., Bottger, A., Zschau, J.: "A new electrode-mesh tomograph for gas-liquid flow" Flow Measurement and Instrumentation, Vol. 9, pp.111-119, 1998.

[14] Prasser, H.-M., Krepper, E., Lucas, D.: "Evolution of the Two-Phase Flow in a Vertical Tube - Decomposition of Gas Fraction Profiles according to Bubble Size Classes using Wire-Mesh Sensors", International Journal of Thermal Sciences, Vol. 41, pp. 17-28, 2002.

[15] Westin J., Alavyoon F, Andersson L., Veber P., Henriksson M., Andersson C.: "Experiments and Unsteady CFD-Calculations of Thermal Mixing in a T-Junction", OECD/NEA/IAEA Workshop on the Benchmarking of CFD Codes for Application to Nuclear Reactor Safety (CFD4NRS), Munich, Germany, 2006, pp. 1-15.

[16] Westin J.: "Thermal Mixing in a T-Junction. Model Tests at Vattenfall research and Development AB 2006. Boundary Conditions and List of Available Data for CFD-Validation", Report Memo U 07-26, Vattenfall R&D AB, Älvkarleby, Sweden, 2007, pp. 1-17.

[17] Westin J., Veber P., Andersson L., 't Mannetje C., Andersson U., Eriksson J., Hendriksson M., Alavyoon F., Andersson C.: "High-Cycle Thermal Fatigue in Mixing Tees. Large-Eddy Simulations Compared to a New Validation Experiment", 16th Int. Conf. On Nuclear Engineering (ICONE-16), Florida, Orlando, USA, 11-15 May 2008, Paper No. 48731, pp. 1-11.

[18] Zboray R., Manera A., Niceno B., Prasser H.-M.: "Investigations on Mixing Phenomena in Single-phase Flows in a T-Junction Geometry", The 12th Int. Topical Meeting on Nuclear Reactor Thermal Hydraulics (NURETH-12), Sheraton Station Square, Pittsburgh, Pennsylvania, U.S.A. September 30-October 4, 2007, Paper No. 71, pp. 1-20.